A joint image dehazing and segmentation model

Haider ALI[1] , **Awal SHER**[1] , **Nosheen ZIKRIA**[2] , **Lavdie RADA**[3,*]

[1]Department of Mathematics, University of Peshawar, Peshawar, Pakistan
[2]Jinnah College for Women, University of Peshawar, Peshawar, Pakistan
[3]Department of Biomedical Engineering, Faculty of Engineering, Bahçeşehir University, İstanbul, Turkey

Abstract: Objects and their feature identification in hazy or foggy weather conditions has been of interest in the last decades. Improving image visualization by removing weather influence factors for easy image postprocessing, such as object detection, has benefits for human assistance systems. In this paper, we propose a novel variational model that will be capable of jointly segmenting and dehazing a given image. The proposed model incorporates atmospheric veil estimation and locally computed denoising constrained surfaces into a level set function by performing a robust and efficient image dehazing and segmentation scheme for both gray and color outdoor images. The proposed model not only shows efficient segmentation of objects in foggy images by outperforming state-of-the-art methods but also produces dehazed object results in the same time.

Key words: Active contours, image dehazing, variational approach, segmentation, Euler–Lagrange equation

1. Introduction

Despite the increasing ubiquity of digital photography, images of outdoor scenes have low visibility due to fog or haze and consecutively recovering the original colors of natural scenes is a hard problem. Augmenting the depth information from images captured with ordinary cameras is still a long-standing unsolved problem in image processing and computer vision. In the last decades, several methods that moderately solve the problem have been proposed [1–4]. Among the earliest dehazing approaches, one can distinguish the polarization filters techniques [5, 6], in which multiple images were required to remove fog from a given scene. Those models have limited applications as most of the imputed data are with only one single haze image. Moreover, this technique does not guarantee absolute removal of fog or haze. To overcome the disadvantage of multiple images in defogging methods, Tan et al. [7] observed that fog-free images have higher contrast in comparison with foggy images. As a straightforward outcome of this observation, they introduced the contrast maximization method. Although this method requires one single image as algorithm input, the restored images of this method often will have halo artifacts and overstretches due to the fact that the method does not conform to physical effects. Further, He et al. [4] proposed an image prior-dark channel model to remove haze from a single input image. The method is based on a key observation that most local patches in outdoor haze-free images contain some pixels whose intensity is very low in at least one color channel. Using this prior with the haze imaging model, one can directly estimate the thickness of the haze and recover high-quality haze-free images. To remove haze, He et al. [4] proposed the following formula:

---

*Correspondence: lavdie.rada@eng.bau.edu.tr

$$I(\mathbf{x})^{dark} = \min_{\mathbf{y} \in \Omega_0(\mathbf{x})} (\min_{c \in (r,g,b)} I^c(\mathbf{y})), \tag{1}$$

where $I^c(\mathbf{x})$ is a color channel of the given image $I(\mathbf{x})$ definite in the domain $\Omega \in \mathcal{R}^2$, and $\Omega_0(\mathbf{x})$ is a local patch with center $\mathbf{x}$. In most of nonsky local image areas, we have

$$I(\mathbf{x})^{dark} = \min_{\mathbf{y} \in \Omega_0(\mathbf{x})} (\min_{c \in (r,g,b)} I^c(\mathbf{y})) = 0. \tag{2}$$

However, the output images of the method may have color tone modification due to imprecise estimation of air/light. Considering the degradation of image quality of outdoor scenes as a process affected by attenuation and the air/light [8], occurring due to the scattering of atmospheric particles [9], this phenomenon can be restored by reversing Koschmieder's law [1], which is given with the following formula:

$$I(\mathbf{x}) = I_0(\mathbf{x})e^{-kd(\mathbf{x})} + I_\infty(\mathbf{x})(1 - e^{-kd(\mathbf{x})}), \tag{3}$$

where $I(\mathbf{x})$ is a given image with fog, $I_0(\mathbf{x})$ is a fog-free image, k is the defunctness coefficient of the fog, $d(\mathbf{x})$ is the distance of the scene point from the photographic equipment at pixel $\mathbf{x}$, and $I_\infty(\mathbf{x})$ is the sky intensity. For homogeneous fog, both $I_\infty(\mathbf{x})$ and k are global constants over the whole image, while for heterogeneous fog it may vary locally. Representing the air/light as $A(\mathbf{x})$, the formula in Eq. (3) can be written as

$$I(\mathbf{x}) = I_0(\mathbf{x})\Big(1 - \frac{A(\mathbf{x})}{I_\infty}\Big) + A(\mathbf{x}). \tag{4}$$

To improve this model, Cho et al. [1] proposed the minimization of the following functional:

$$E(A(\mathbf{x})) = \int_\Omega (H(W(\mathbf{x}) - A(\mathbf{x}))d\mathbf{x} + \lambda^2 \int_\Omega \varphi(||\nabla A(\mathbf{x})||)d\mathbf{x}, \tag{5}$$

where Ω is the domain of the given image, $A(\mathbf{x})$ is air/light or atmospheric veil, $W(\mathbf{x}) = min(I(\mathbf{x}))$ is the minimum components of $I(\mathbf{x})$ for each pixel (image of the whiteness within the observed image), H is the Heaviside function, λ is a regularization parameter that balances the influence between two terms of Eq. (4), and φ represents an edge-preserving regularization function (assumed to be an even function in $\mathcal{C}^2(\mathcal{R})$). This model outperformed the existing image dehazing algorithms by not only showing good results for image restoration in heavy fog but at the same time by not producing halo effects. To improve the performance of the model of Cho et al. [1], several works have been introduced in recent years [10–13]. However, these models and other similar models [2–4] may not work properly in multiple image dehazing cases.

On the other hand, segmentation of a given image refers to the process of locating objects and boundaries (lines, curves, etc.) in images. The most popular and successful methods for image segmentation are active contour approaches. Those techniques can be classified into two groups: edge-based [14–18] and region-based [19, 20, 28] models. The choice of these models depends on results' acceptability for every image and problem in each specific segmentation application. In comparison with edge-based methods, the region-based active contour frameworks are well known for their correctness in segmenting images with or without noise with or without gradient. The Chan–Vese (CV) model is one of the most popular region-based active contour models [19], which is obtained due to the minimization of the following functional:

$$F^{CV}(c_1, c_2, C) = \mu \, length(C) + \lambda_1 \int_{inside(C)} |I(\mathbf{x}) - c_1|^2 d\mathbf{x} + \lambda_2 \int_{outside(C)} |I(\mathbf{x}) - c_2|^2 d\mathbf{x},$$

where λ_1, λ_2 are positive constants and c_1, c_2 are average intensities inside and outside of the contour C, respectively. Representing contour C with a zero level set, i.e. $C = \{\mathbf{x} \in \Omega | \phi(\mathbf{x}) = 0\}$, and minimizing the above energy functional with respect to ϕ, c_1, and c_2, we obtain the following variational formulation:

$$\delta_\epsilon(\phi)\left[\mu\nabla.\left(\frac{\nabla\phi}{|\nabla\phi|}\right) - \lambda_1(I(\mathbf{x}) - c_1)^2 + \lambda_2(I(\mathbf{x}) - c_2)^2\right] = 0, \tag{6}$$

$$c_1 = \frac{\int_\Omega I(\mathbf{x})H(\phi(\mathbf{x}))d\mathbf{x}}{\int_\Omega H(\phi(\mathbf{x}))d\mathbf{x}}, \text{ and } c_2 = \frac{\int_\Omega I(\mathbf{x})(1 - H(\phi(\mathbf{x})))d\mathbf{x}}{\int_\Omega (1 - H(\phi(\mathbf{x})))d\mathbf{x}}. \tag{7}$$

The drawback of the CV model is its deficiency in segmenting images with inhomogeneous intensity, including fog and haze. To improve the CV model, Li et al. [21] proposed a local binary fitting (LBF) energy model, which is capable of segmenting images with intensity inhomogeneity. The LBF energy embedding the variational model is given by:

$$F^{LBF}(C, f_1, f_2) = \mu length(C) + \lambda_1 e_1 + \lambda_2 e_2 \tag{8}$$

with

$$e_1 = \int K_\sigma(\mathbf{x} - \mathbf{y})|I(\mathbf{y}) - f_1(\mathbf{x})|^2 H(\phi(\mathbf{y})d\mathbf{y}, \tag{9}$$

$$e_2 = \int K_\sigma(\mathbf{x} - \mathbf{y})|I(\mathbf{y}) - f_2(\mathbf{x})|^2 (1 - H(\phi(\mathbf{y}))d\mathbf{y},$$

where ϕ is a level set function, $H(\phi)$ is the Heaviside function, $K_\sigma(\mathbf{x}) = \frac{1}{(2\pi)^{n/2}\sigma^2}.e^{-|\mathbf{x}|^2/2\sigma^2}$ is the Gaussian kernel, and f_1 and f_2 are two smooth functions that approximate the local image intensities inside and outside contour C, respectively. Minimization of the above equation with respect to ϕ, f_1, and f_2 leads to the following equations:

$$\delta_\epsilon(\phi)\left[\mu\nabla.\left(\frac{\nabla\phi}{|\nabla\phi|}\right) - (\lambda_1 e_1 - \lambda_2 e_2)\right] = 0, \tag{10}$$

$$f_1(\mathbf{x}) = \frac{K_\sigma(\mathbf{x}) * I(\mathbf{x})H_\epsilon(\phi(\mathbf{x}))}{K_\sigma(\mathbf{x}) * H_\epsilon(\phi(\mathbf{x}))}, \text{ and } f_2(\mathbf{x}) = \frac{K_\sigma(\mathbf{x}) * I(\mathbf{x})(1 - H_\epsilon(\phi(\mathbf{x})))}{K_\sigma(\mathbf{x}) * (1 - H_\epsilon(\phi(\mathbf{x})))}. \tag{11}$$

Similar work was recently introduced by Zhang et al. [27]. The proposed model incorporates a local image fitting (LIF) term for segmentation. Their proposed energy functional is as follows:

$$E^{LIF}(\phi) = \mu length(C) + \frac{1}{2}\int_\Omega |I(\mathbf{x}) - I_0'(\mathbf{x})|^2 d\mathbf{x}, \tag{12}$$

where

$$I_0'(\mathbf{x}) = m_1 H_\epsilon(\phi(\mathbf{x})) + m_2(1 - H_\epsilon(\phi(\mathbf{x}))) \tag{13}$$

represents the local computed image and m_1 and m_2 are the local averages given by:

$$m_1 = mean(z_0 \in (\{\mathbf{x} \in \Omega : \phi(\mathbf{x}) < 0\}\bigcap W_\sigma(\mathbf{x}))), \tag{14}$$

$$m_2 = mean(z_0 \in (\{\mathbf{x} \in \Omega : \phi(\mathbf{x}) > 0\}\bigcap W_\sigma(\mathbf{x}))), \tag{15}$$

with $W_\sigma(\mathbf{x})$ a rectangular window function. The window function can be chosen in different ways, e.g., a truncated Gaussian window or a constant window. In can be easily noticed that in the case where $W_\sigma(\mathbf{x})$ is a truncated Gaussian window then m_1 and m_2 are equal to f_1 and f_2 in Eq. (10).

Another attempt to enhance the CV model was made by Wu et al. [22], who proposed the following energy functional:

$$F(\phi) = \lambda \int \frac{(I(\mathbf{x}) - c_1)^2}{c_1^2} (\phi + 1)^2 d\mathbf{x} + \int \frac{(I(\mathbf{x}) - c_2)^2}{c_2^2} (\phi - 1)^2 d\mathbf{x}, \tag{16}$$

where c_1, c_2 are constants and $\lambda > 0$. The proposed variational segmentation model is convex with unique global solution for its energy functional within the interval $[-1, 1]$.

Furthermore, Zhang et al. [27] combined the region base idea introduced by Chan and Vese [19] with a geodesic model idea and formulated the following minimization functional in terms of level set formulation:

$$\frac{\partial \phi(\mathbf{x})}{\partial t} = \alpha(SPF)|\nabla \phi(\mathbf{x})|, \text{ in } \Omega,$$

$$\phi(t = 0; \mathbf{x}) = \phi_0(\mathbf{x}), \text{ in } \Omega,$$

where SPF denotes the signed pressure force function, α is a positive constant, and ϕ_0 is the initial level set function. Akram et al. [23] modified the Zhang model for images with intensity inhomogeneity by replacing the SPF function with a local SPF function. Although Akram et al. [23] improved the performance of the region-based active contour models by efficiently stopping the contours at weak or blurred edges, the model is not designed to handle images having multiple intensity objects. To improve the local SPF model, Ali et al. [24] proposed a combination of the SPF function with the generalized average concept in a new segmentation framework. Their model is given as follows:

$$\frac{\partial \phi(\mathbf{x})}{\partial t} = \alpha(GSPF)|\nabla \phi(\mathbf{x})|, \text{ in } \Omega,$$

$$\phi(t = 0; \mathbf{x}) = \phi_0(\mathbf{x}), \text{ in } \Omega.$$

The model shows significant improvements over the model of [23] for segmentation of multiregion images with inhomogeneous intensities. To the best of our knowledge, there is no single designed model to jointly segment and dehaze images with fog or haze.

In this work, we propose a novel variational model that will be capable of jointly segmenting and dehazing a given image at the same time. Our model is mainly based on estimating the atmospheric veil and level set function for efficient image dehazing and segmentation, respectively. Most of the recent image segmentation models may not efficiently segment foggy images. The proposed technique is robust for both gray and color outdoor images. The experimental tests of our proposed method on color and gray images will validate that our formulation is far better than the latest segmentation techniques available in the literature.

2. The proposed model

Let $I(\mathbf{x})$ denote the given image with fog factor over a domain Ω, $I : \Omega \subset R^2 \longrightarrow R$, and its statistically locally computed approximated image $I_f(\mathbf{x})$ is as follows:

$$I_f(\mathbf{x}) = f_1(\mathbf{x})H_\epsilon(\phi(\mathbf{x})) + f_2(\mathbf{x})(1 - H_\epsilon(\phi(\mathbf{x})), \tag{17}$$

where $f_1(\mathbf{x})$ and $f_2(\mathbf{x})$ are smooth functions similarly obtained as in Eq. (10). Both terms will statistically contain significant information under haze and fog conditions contrary to global fitting terms such as c_1 and c_2 for the CV model.

In order to jointly dehaze and segment a given image, we propose the following energy functional:

$$E(\phi(\mathbf{x}), A(\mathbf{x})) = \int_\Omega |\nabla A(\mathbf{x})| d\mathbf{x} + \lambda^2 \int_\Omega H(\phi(\mathbf{x}))(W(\mathbf{x}) - A(\mathbf{x})) d\mathbf{x} +$$

$$\mu \int_\Omega \delta(\phi(\mathbf{x})) |\nabla \phi(\mathbf{x})| d\mathbf{x} +$$

$$\lambda_1 \int_\Omega (I_f(\mathbf{x}) - I_A(\mathbf{x}))^2 d\mathbf{x} + (1 - \lambda_1) \int_\Omega (log I_f(\mathbf{x}) + \frac{I_A(\mathbf{x})}{I_f(\mathbf{x})}) d\mathbf{x}, \tag{18}$$

where μ, λ_1, and λ are positive parameters. The first and the second terms of Eq. (18) represent the physical properties of the atmospheric veil. Atmospheric veil $A(\mathbf{x})$ is an increasing function of the scene point distance $d(\mathbf{x}, \mathbf{y})$, whereas $A(\mathbf{x})$ is positive and higher than the minimum of the components of $I(\mathbf{x})$ [1]. This imposes the smoothness of the air/light $A(\mathbf{x})$ everywhere into the image domain, positivity $A(\mathbf{x}) \geq 0$, and $A(\mathbf{x}) < W(\mathbf{x})$, where $W(\mathbf{x}) = min(I(\mathbf{x}))$. The other terms in Eq. (18) are variational segmentation fitting and smoothness terms for the curve fitting where $I_A(\mathbf{x})$ is given by:

$$I_A(\mathbf{x}) = \frac{I(\mathbf{x}) - A(\mathbf{x})}{1 - \frac{A(\mathbf{x})}{I_\infty(\mathbf{x})}}. \tag{19}$$

In other words, the first two terms of the proposed energy function satisfy the edge-preserving regularization property while adequately removing fog, whereas the last three terms will evolve the curve ϕ towards an object's boundary. Minimizing the energy functional $E(\phi(\mathbf{x}), A(\mathbf{x}))$ with respect to $\phi(\mathbf{x})$, we will get the following equation:

$$\mu \delta(\phi(\mathbf{x})) \nabla(\frac{\nabla \phi(\mathbf{x})}{|\nabla \phi(\mathbf{x})|}) + 2\lambda_1 (I_A(\mathbf{x}) - I_f(\mathbf{x}))(-f_1(\mathbf{x}) \delta(\phi(\mathbf{x})) + f_2(\mathbf{x}) \delta(\phi(\mathbf{x})))$$

$$+(1 - \lambda_1)(\frac{1}{I_f(\mathbf{x})}(f_1(\mathbf{x}) \delta(\phi(\mathbf{x})) - f_2(\mathbf{x}) \delta(\phi(\mathbf{x}))) + \frac{I_A(\mathbf{x})}{I_f^2(\mathbf{x})}(f_1(\mathbf{x}) \delta(\phi(\mathbf{x})) - f_2(\mathbf{x}) \delta(\phi(\mathbf{x}))) = 0. \tag{20}$$

Eq. (20) can be rewritten as

$$\mu \delta(\phi(\mathbf{x})) \nabla(\frac{\nabla \phi(\mathbf{x})}{|\nabla \phi(\mathbf{x})|}) + (f_1(\mathbf{x}) \delta(\phi(\mathbf{x})) - f_2(\mathbf{x}) \delta(\phi(\mathbf{x}))) \Big[-2\lambda_1(I_A - I_f) + (1 - \lambda_1)(\frac{1}{I_f} + \frac{I_A}{I_f^2}) \Big] = 0.$$

Using the time marching method to solve the above equation we get the following evolution equation:

$$\frac{\partial \phi(\mathbf{x})}{\partial t} = \delta(\phi(\mathbf{x})) \Big[\mu \nabla(\frac{\nabla \phi(\mathbf{x})}{|\nabla \phi(\mathbf{x})|}) + (f_1(\mathbf{x}) - f_2(\mathbf{x})) [\frac{(1 - \lambda_1)}{I_f^2}(I_f + I_A) - 2\lambda_1(I_A - I_f)] \Big]. \tag{21}$$

In a similar way, minimizing the energy functional $E(\phi(\mathbf{x}), A(\mathbf{x}))$ with respect to A($\mathbf{x}$), we derive the following equation:

$$\nabla \Big(\frac{\nabla A}{|\nabla A|} \Big) - \lambda^2 \delta(\phi)(W - A) + \frac{2\lambda_1}{(1 - \frac{A}{I_\infty})^3}(\frac{I}{I_\infty} - 1)\Big(I - A - I_f(1 - \frac{A}{I_\infty})\Big) - \frac{(1 - \lambda_1)}{I_f(1 - \frac{A}{I_\infty})^2}(\frac{I}{I_\infty} - 1) = 0.$$

Rewriting the above equation, we obtain:

$$\nabla\Big(\frac{\nabla A}{|\nabla A|}\Big) - \lambda^2\delta(\phi)(W - A) + \frac{(\frac{I}{I_\infty} - 1)}{(1 - \frac{A}{I_\infty})^2}\Big[\frac{2\lambda_1}{1 - \frac{A}{I_\infty}}\Big(I - A - I_f(1 - \frac{A}{I_\infty})\Big) - \frac{1 - \lambda_1}{I_f}\Big] = 0,$$

and its evolution equation,

$$\frac{\partial A}{\partial t} = \nabla\Big(\frac{\nabla A}{|\nabla A|}\Big) - \lambda^2\delta(\phi)(W - A) + \frac{(\frac{I}{I_\infty} - 1)}{(1 - \frac{A}{I_\infty})^2}\Big[\frac{2\lambda_1}{1 - \frac{A}{I_\infty}}\Big(I - A - I_f(1 - \frac{A}{I_\infty})\Big) - \frac{1 - \lambda_1}{I_f}\Big]. \qquad (22)$$

2.1. Numerical implementation

Shortly rewriting Eq. (21), we have

$$\frac{\phi(\mathbf{x})}{\partial t} = K(\phi(\mathbf{x})),$$

where $K(\phi(\mathbf{x}))$ is the right-hand side in Eq. (21). Considering Ω as a two-dimensional space and using the finite differences for the discretization of Eq. (21), we obtain:

$$\frac{\phi_{i,j}^{n+1} - \phi_{i,j}^n}{\Delta t} = K(\phi_{i,j}^n).$$

In other words,

$$\phi_{i,j}^{n+1} = \phi_{i,j}^n + \Delta t\delta(\phi^n)\Big[\mu\kappa_\phi + (f_1 - f_2)[\frac{(1 - \lambda_1)}{I_f^2}(I_f + I_A) - 2\lambda_1(I_A - I_f)]\Big], \qquad (23)$$

where κ_ϕ represents the curvature and is computed according to the following formula:

$$\kappa_\phi = div(\frac{\nabla\phi}{|\nabla\phi|}) = \frac{\phi_{xx}\phi_y^2 - 2\phi_{xy}\phi_x\phi_y + \phi_{yy}\phi_x^2}{(\phi_x^2 + \phi_y^2)^{3/2}} \qquad (24)$$

where ϕ_x, ϕ_y, ϕ_{xx}, ϕ_{yy}, and ϕ_{xy} are computed as follows:

$$\phi_x = \frac{1}{2h}(\phi_{i+1,j} - \phi_{i-1,j}), \ \phi_y = \frac{1}{2h}(\phi_{i,j+1} - \phi_{i,j-1}),$$

$$\phi_{xx} = \frac{1}{h^2}(\phi_{i+1,j} + \phi_{i-1,j} - 2\phi_{i,j}), \ \phi_{yy} = \frac{1}{h^2}(\phi_{i,j+1} + \phi_{i,j-1} - 2\phi_{i,j}),$$

$$\phi_{xy} = \frac{1}{h^2}(\phi_{i+1,j+1} - \phi_{i-1,j+1} - \phi_{i+1,j-1} + \phi_{i-1,j-1}), \qquad (25)$$

where h is the grid point.

In a similar way, Eq. (22) can be discretized as follows:

$$\frac{A_{i,j}^{n+1} - A_{i,j}^n}{\Delta t} = R(A_{i,j}^n),$$

where $R(A_{i,j}^n)$ is the right-hand side in Eq. (22) and $\kappa_A = div(\frac{\nabla A}{|\nabla A|})$ can be written in a similar form as follows:

$$\kappa_A = div(\frac{\nabla A}{|\nabla A|}) = \frac{A_{xx}A_y^2 - 2A_{xy}A_xA_y + A_{yy}A_x^2}{(A_x^2 + A_y^2)^{3/2}}, \qquad (26)$$

where A_x, A_y, A_{xx}, A_{yy}, and A_{xy} are computed as:

$$A_x = \frac{1}{2h}(A_{i+1,j} - A_{i-1,j}), \; A_y = \frac{1}{2h}(A_{i,j+1} - A_{i,j-1}),$$

$$A_{xx} = \frac{1}{h^2}(A_{i+1,j} + A_{i-1,j} - 2A_{i,j}), \; A_{yy} = \frac{1}{h^2}(A_{i,j+1} + A_{i,j-1} - 2A_{i,j}),$$

$$A_{xy} = \frac{1}{h^2}(A_{i+1,j+1} - A_{i-1,j+1} - A_{i+1,j-1} + A_{i-1,j-1}), \tag{27}$$

$$A_{i,j}^{n+1} = A_{i,j}^n + \Delta t\Big(\kappa_A - \lambda^2 \delta(\phi^n)(W - A_{i,j}^n),$$

$$+\frac{(\frac{I}{I_\infty} - 1)}{(1 - \frac{A_{i,j}^n}{I_\infty})^2}\Big[\frac{2\lambda_1}{1 - \frac{A_{i,j}^n}{I_\infty}}\Big(I - A_{i,j}^n - I_f(1 - \frac{A_{i,j}^n}{I_\infty})\Big) - \frac{1 - \lambda_1}{I_f}\Big]\Big). \tag{28}$$

In the following we show some basic steps of our algorithm.

Algorithm 1 Joint segmentation dehazing method algorithm: $(\phi^k(\mathbf{x}), A^k(\mathbf{x})) \leftarrow JDS(\phi^{(k-1)}, A^{(k-1)}, \mu, \lambda_1, \lambda_2, \epsilon, max_{iter}, tol)$.

---

1. Initialize the level function $\phi(x)$ by $\phi_0(x)$ and A^0 by A_0.

$$A^0(\mathbf{x}) = \beta I(\mathbf{x}), 0 < \beta < 1,$$

and the level set function $\phi(\mathbf{x})$ with $\phi^0(\mathbf{x})$

$$\phi^0 = \phi(\mathbf{x}, t = 0) = \begin{cases} -\rho & \text{if } \mathbf{x} \in \Omega - \partial\Omega \\ 0 & \text{if } \mathbf{x} \in \partial\Omega \\ \rho & \text{if } \mathbf{x} \in \Omega - \Omega \end{cases}$$

where $\rho > 0$ is a constant, Ω is image domain, and $\partial\Omega$ is the boundary of Ω.
2. Calculate $f_1^k(\mathbf{x})$ and $f_2^k(\mathbf{x})$ using Eq. (10).
3. Update $\phi(\mathbf{x})^k$, Eq. (21), using its discretization, Eq. (23).
4. Update $A(\mathbf{x})^k$, Eq. (22), using its discretization, Eq. (23).
5. Check whether the solution is stationary. If not, repeat from Step 2.

---

3. Experimental results

In this section, we display the results obtained from our model for foggy images of various scenes and show that the model can easily handle dehazing and segmentation by outperforming other existing models. Simulation and performance evaluation of the proposed algorithm is accomplished with various clean and foggy images on the MATLAB platform in the Windows 8.1 environment and Intel core i3 environment on a 1.70 GHz personal computer with 4.00 GB installed memory (RAM). For both gray and color images, we fixed the parameters $\lambda_1 = 0.01$, $\lambda_2 = 100$, $\mu = 0.02$, and $max_{iter} = 100$. To achieve better results the parameters can be tuned depending on the fog/haze level, or, alternatively, an optimized scheme can be found.

3.1. Dehazing comparison with existing models

In the first test set we show the capability of the proposed model in fog removal. Figure 1 shows defogging results of the proposed method applied on different images and compared with the state of the art of Ancuti et

al. [25] and Cho et al. [1] models. From the experimental results, in this figure we witness a robust performance in restoring the given image and clearly observe the correctness of the proposed method in terms of dehazing outdoor images. The proposed algorithm shows clear details of fog-free scene objects as compared to other methods in images with intense fog. The obtained results have acceptable visual quality without sky region or less sky region.
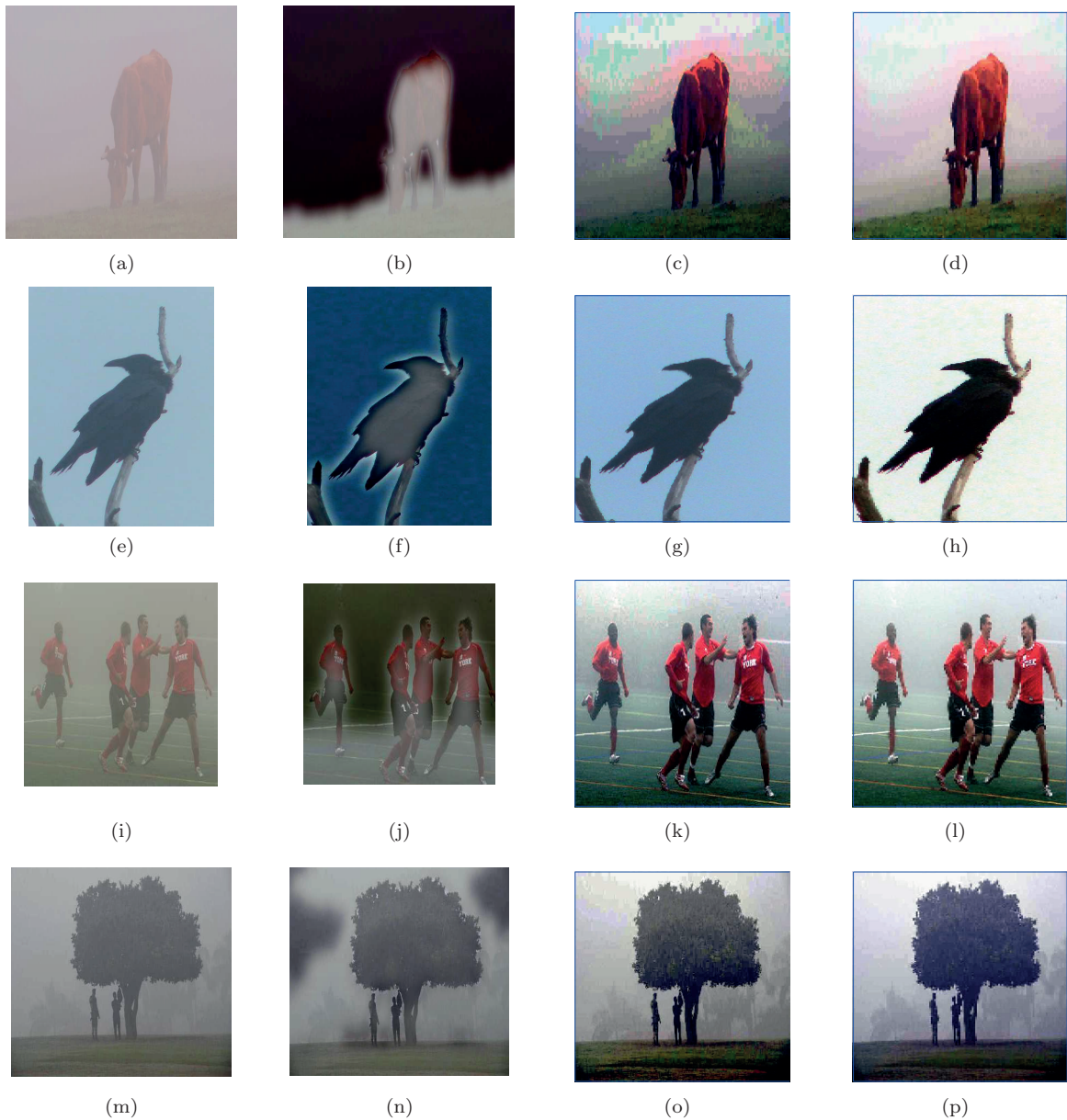

(a)　　　　　　　　(b)　　　　　　　　(c)　　　　　　　　(d)

(e)　　　　　　　　(f)　　　　　　　　(g)　　　　　　　　(h)

(i)　　　　　　　　(j)　　　　　　　　(k)　　　　　　　　(l)

(m)　　　　　　　　(n)　　　　　　　　(o)　　　　　　　　(p)

Figure 1. The defogging performance of the proposed model in comparison with the models of Ancuti et al. [25] and Cho et al. [1]. The first column is the given image, the second column shows the output results of the Ancuti [25] model, the third column shows the output results of the Cho [1] model, and the fourth column shows the results of the proposed model.

3.2. Segmentation accuracy of the proposed method for clean images and its comparison with state of art models

In order to show the segmentation performance of the proposed model we test the model on gray and color clean images. Figures 2 and 3 show the obtained results of the proposed method in comparison with the segmentation performance of the SPF [26] and GSPF [24] models. As expected, the application of the LBF model to the same set of images gives similar results as the proposed method, not being repetitive. From the experimental results we notice that our method performs well in segmenting gray and vector-valued images, whereas the other methods have similar results. The experiments carried out in this test set are followed by experiments with images containing fog and their comparative quantitative analysis on coupled dehaze and segmentation.
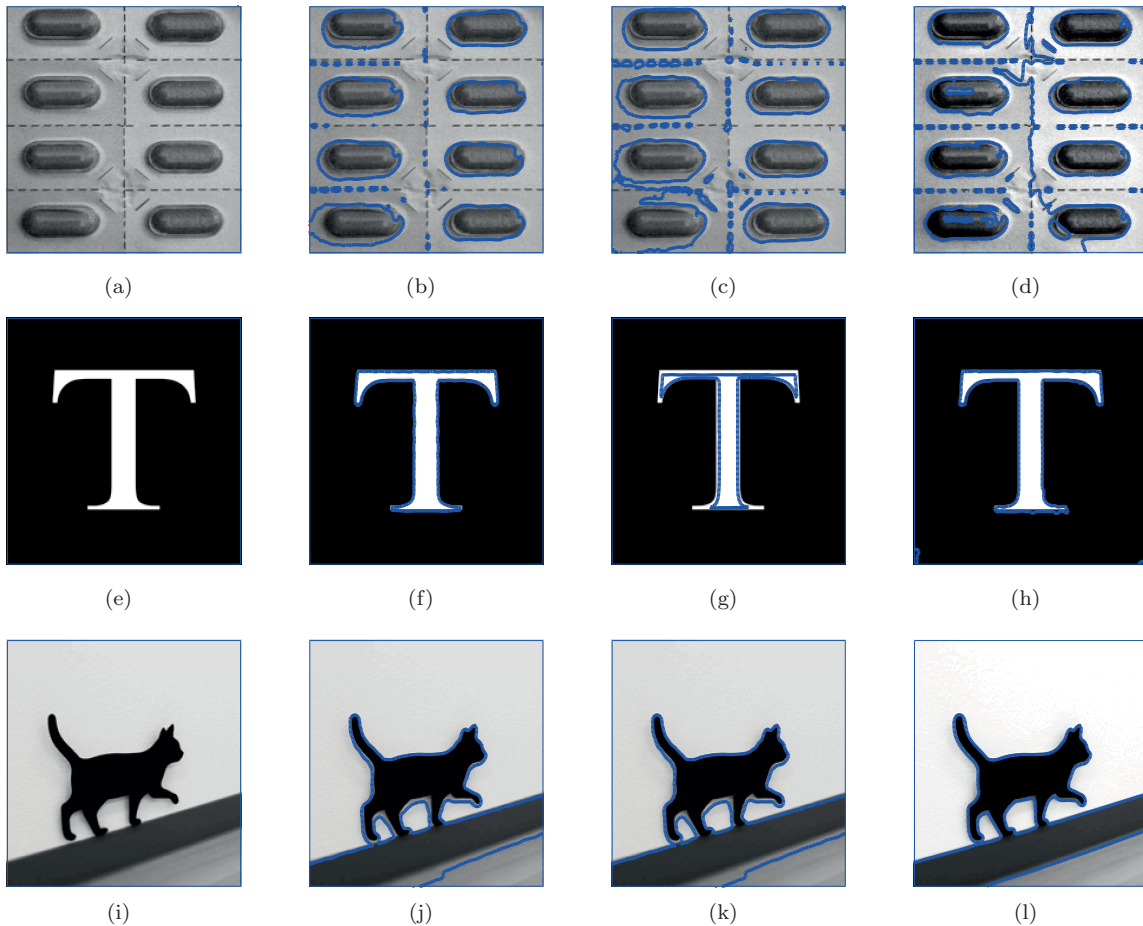
(a)	(b)	(c)	(d)
(e)	(f)	(g)	(h)
(i)	(j)	(k)	(l)

Figure 2. The first column is the given gray image, the second column shows the local SPF results [26], the third column shows GSPF results [24], and the fourth column shows the result of our method.

3.3. Segmentation accuracy for fog/haze images and its comparison with state-of-the-art segmentation models

This test set shows the ability of our model to remove fog while segmenting the object of the given image. The results obtained in Figure 4 and Figure 5, show that the proposed model successfully segmented the natural fog images (last columns of Figures 4 and 5). The experiments are carried out on different numbers of scenes containing low and high levels of fog/haze. In these figures we simultaneously compare the performance of
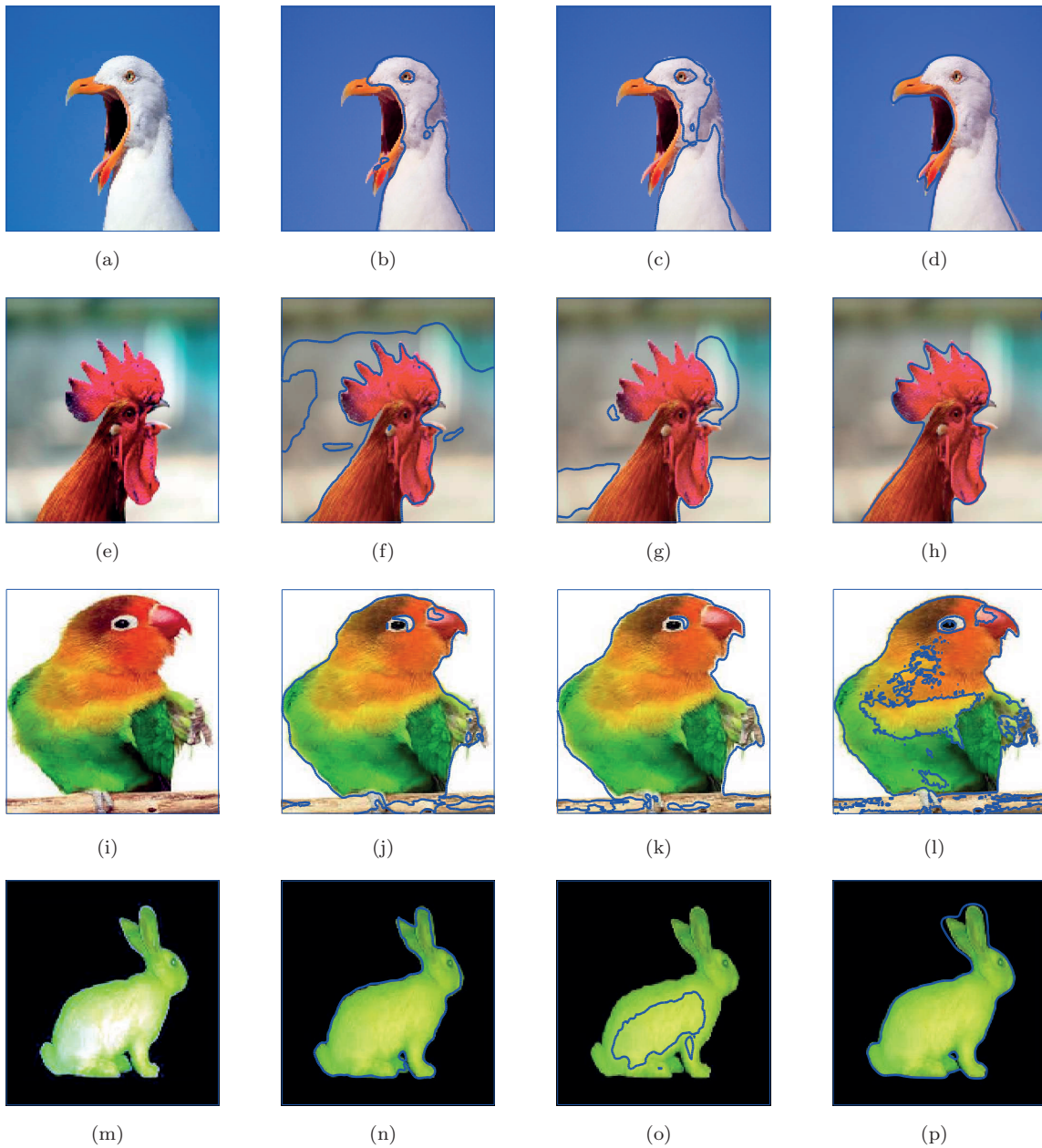
Figure 3. The first column is the given vector-valued image, the second column shows the local SPF results [26], the third column shows GSPF results [24], and the fourth column shows the result of our method.

the proposed method in terms of segmentation with state-of-the-art models such as LBF [21] and the Wu [22] model. The incorporation of the physical properties of the atmospheric veil into the proposed variational model and the representation of the given image as a piecewise continuous function clearly make the proposed method outperform the existing models, which can not cope with such cases. From Figures 4 and 5, in the second and third columns we notice that LBF [21] and the Wu [22] model will give poor results or even wrong results if the scene of the image contains a relatively high level of fog and the foreground objects fall into intensity variation.

(a) Initial Contour　　　　　(b) LBF Results　　　　　(c) Wu Results　　　　　(d) Proposed Method Results

Figure 4. The performance of the proposed model in comparison with LBF (iteration $= 3000$, $\lambda 1 = 1$, $\lambda 2 = 1$) and Wu (iteration $= 5000$) models on images with fog.

3.4. Quantitative analysis

To show the segmentation accuracy of the proposed model we use the Jaccard similarity (JS) coefficient for quantitative comparison of different models, which is defined as the ratio of the junction of the areas and the union. Let $\mathbf{R_1}$ and $\mathbf{R_2}$ denote the segmentation result and ground truth (GT), respectively. Then the **JS** coefficient is computed in the following way:
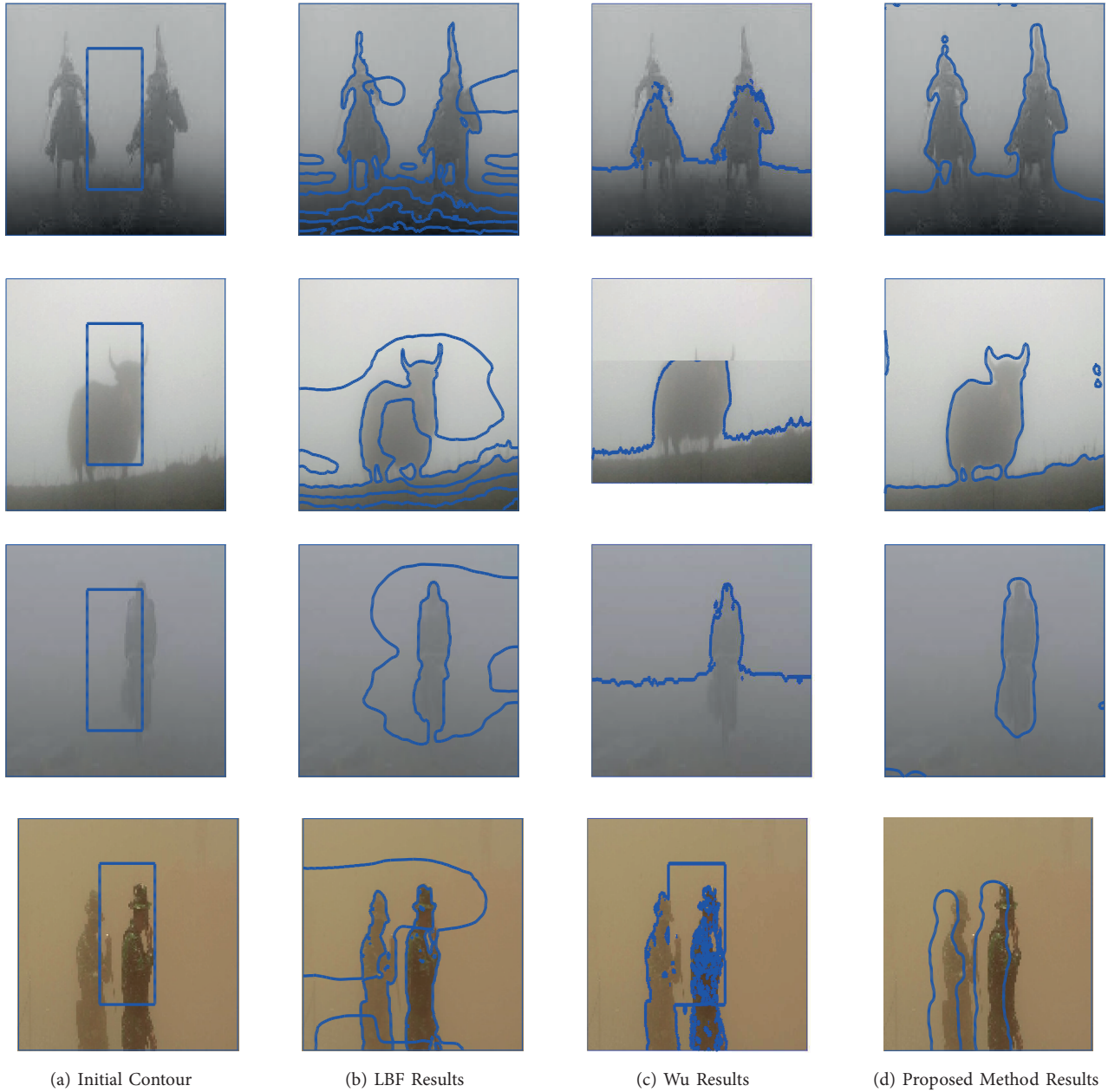
<table>
<tr><td>(a) Initial Contour</td><td>(b) LBF Results</td><td>(c) Wu Results</td><td>(d) Proposed Method Results</td></tr>
</table>

Figure 5. The performance of the proposed model in comparison with LBF (iteration $= 3000$, $\lambda 1 = 1$, $\lambda 2 = 1$) and Wu (iteration $= 5000$) models on images with fog.

$$\mathbf{JS(R_1, R_2)} = \frac{\mathbf{R_1 \bigcap R_2}}{\mathbf{R_1 \bigcup R_2}}.$$

Clearly, the values of **JS** coefficients are $\mathbf{JS} \in [\mathbf{0, 1}]$. The accuracy of a model is better if the **JS** coefficient is closer to one and vice versa if **JS** is closer to zero. Figure 6 compares the **JS** coefficients obtained by LBF [21], the Wu model [22], and the proposed method obtained over time, presented in the second, third, and last columns, respectively. We easily observe that the proposed model performs better in comparison with the other
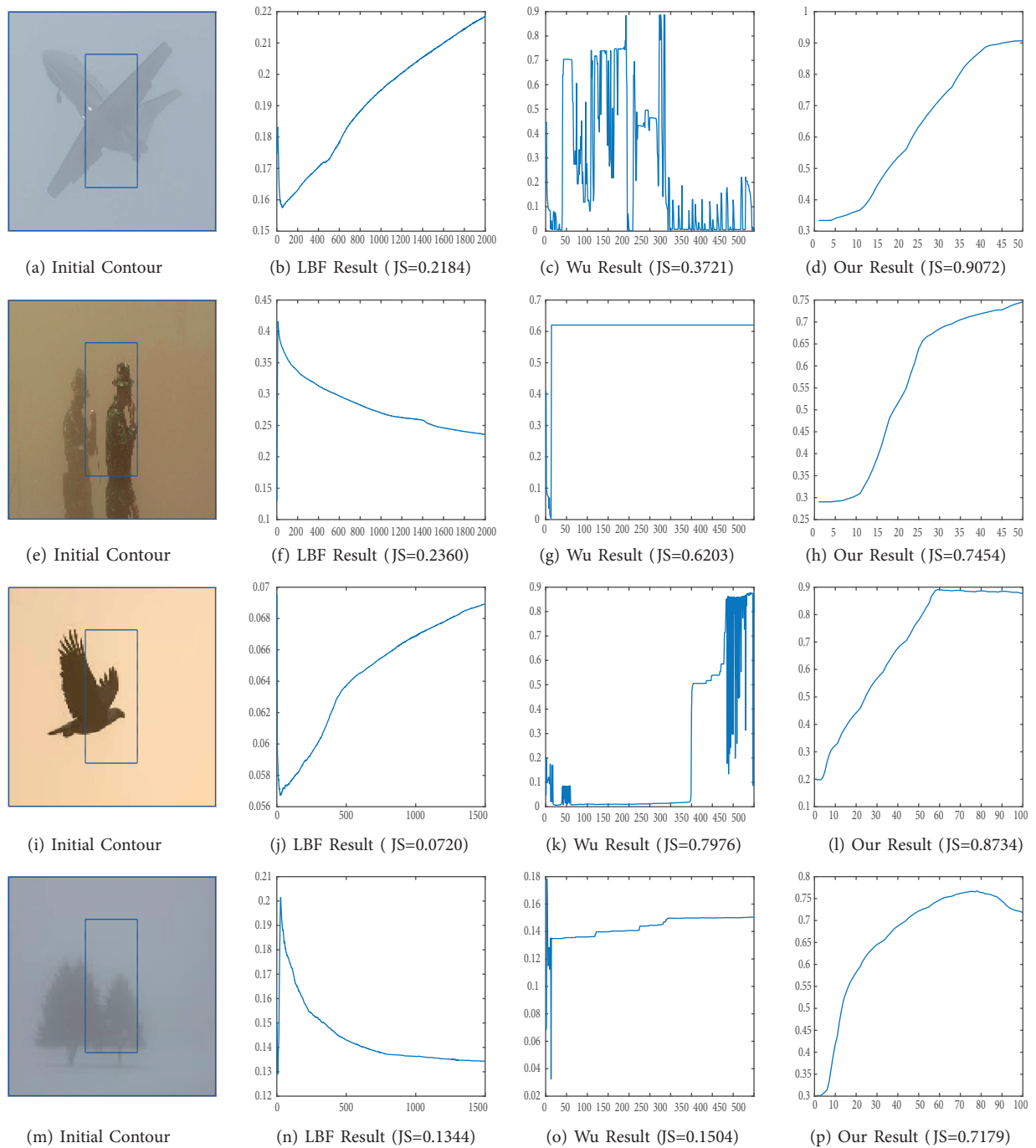
(a) Initial Contour   (b) LBF Result (JS=0.2184)   (c) Wu Result (JS=0.3721)   (d) Our Result (JS=0.9072)

(e) Initial Contour   (f) LBF Result (JS=0.2360)   (g) Wu Result (JS=0.6203)   (h) Our Result (JS=0.7454)

(i) Initial Contour   (j) LBF Result (JS=0.0720)   (k) Wu Result (JS=0.7976)   (l) Our Result (JS=0.8734)

(m) Initial Contour   (n) LBF Result (JS=0.1344)   (o) Wu Result (JS=0.1504)   (p) Our Result (JS=0.7179)

Figure 6. Quantitative analysis using JS coefficients for comparison between LBF, Wu, and proposed method.

models. The proposed algorithm produces higher JS values as compared to other state-of-the-art methods for most of the images tested. Higher values of JS show better accuracy, which indicates a good performance of the proposed model. Moreover, the graphs showing the **JS** coefficients reveal robustness and stability of the performance of the proposed model, whereas the other methods cannot cope with such images. This is to be expected as none of the methods mentioned above or other methods in the literature take fog/haze into account.

4. Conclusions

In this paper, we presented an efficient variational segmentation under dehazing image reconstruction in a single combined model. The proposed model jointly segments and dehazes a given image by combining active contour on a region based on image segmentation with a variational level set formulation. To recover the boundary of the desired object we introduce local binary fitting energy terms as well as edge-preserving regularization to utilize accurate air/light maps. The model is applicable for both gray and color images. Experimental results show that our new approach performs well in the comparison with other existing classical models. Moreover, the proposed model has a simple structure and can easily be adapted for special cases such as inhomogeneous fog/haze.

References

[1] Cho WS, Na IS, Seo SC, Kim SK, Park SY. Single image defogging method using variational approach for edge-preserving regularization. World Academy of Science, Engineering, and Technology International Journal of Computer, Electrical, Automation, Control, and Information Engineering 2013; 7: 829-833.

[2] Zhang S, Yao J. Single image dehazing using fixed points and nearest-neighbor regularization. Lecture Notes in Computer Science 2017; 10116: 18-33.

[3] Zhang S, Yao J, Chen CS. Contrast enhancement based single image dehazing via TV-l1minimization. In: 2014 IEEE International Conference on Multimedia and Expo; 2014. pp. 1-6. doi: 10.1109/ICME.2014.6890277

[4] He K, Sun J, Tang X. Single image haze removal using dark channel prior. IEEE Transactions on Pattern Analysis and Machine Intelligence 2011; 33: 2341-2353. doi: 10.1109/TPAMI.2010.168

[5] Shwartz S, Namer E, Schechner YY. Blind haze separation. In: IEEE Computer Society Conference on Computer Vision and Pattern Recognition; 2006. pp. 1984-1991. doi: 10.1109/CVPR.2006.71

[6] Schechner YY, Narasimhan SG, Nayar SK. Instant dehazing of images using polarization. In: Proceedings of the 2001 IEEE Computer Society Conference on Computer Vision and Pattern Recognition; 2001. pp. I-325-I-332. doi: 10.1109/CVPR.2001.990493

[7] Tan RT. Visibility in bad weather from a single image. In: IEEE Computer Society Conference on Computer Vision and Pattern Recognition; 2008. pp. 1-8.

[8] Anwar MT, Khosla A. Vision enhancement through single image fog removal. Engineering Science and Technology International Journal 2017; 20: 1075-1083.

[9] Saggu MK, Singh S. A review on various haze removal techniques for image processing. International Journal of Current Engineering and Technology 2015; 5: 1500-1505.

[10] Fattal R. Dehazing using color-lines. ACM Transactions on Graphics 2014; 34: 13:1-13:14. doi: 10.1145/2651362

[11] Zhu Q, Mai J, Shao L. A fast single image haze removal algorithm using color attenuation prior. IEEE Transactions on Image Processing 2015; 24: 3522-3533. doi: 10.1109/TIP.2015.2446191

[12] Kaplan NH, Ayten KK, Dumlu A. Single image dehazing based on multiscale product prior and application to vision control. Signal, Image and Video Processing 2017; 11: 1389-1396. doi: 10.1007/s11760-017-1097-4

[13] Cai B, Xu X, Jia K, Qing C, Tao D. DehazeNet: An end-to-end system for single image haze removal. Transactions on Image Processing 2016; 25: 5187-5198. doi: 10.1109/TIP.2016.2598681

[14] Caselles V, Kimmel R, Sapiro G. Geodesic active contours. International Journal of Computer Vision 1997; 22: 61-79.

[15] Malladi R, Sethian JA, Vemuri BC. Shape modeling with front propagation: a level set approach. IEEE Transactions on Pattern Analysis and Machine Intelligence 1995; 17: 158-175.

[16] Kimmel R, Amir A, Bruckstein AM. Finding shortest paths on surfaces using level sets propagation. IEEE Transactions on Pattern Analysis and Machine Intelligence 1995; 17: 635-640. doi: 10.1109/34.387512

[17] Li C, Xu C, Gui C, Fox MD. Level set evolution without re-initialization: a new variational formulation. In: IEEE Computer Society Conference on Computer Vision and Pattern Recognition; 2005. pp. 430-436. doi: 10.1109/CVPR.2005.213

[18] Kass M, Witkin A, Terzopoulos D. Snakes: Active contour models. International Journal of Computer Vision 1988; 1: 321-331. doi: 10.1007/BF00133570

[19] Chan TC, Vese L. Active contours without edges. IEEE Transactions on Image Processing 2001; 10: 266-277. doi: 10.1109/83.902291

[20] Tsai A, Yezzi A, Willsky AS. Curve evolution implementation of the Mumford-Shah functional for image segmentation, denoising, interpolation, and magnification. IEEE Transactions on Image Processing 2001; 10: 1169-1186. doi: 10.1109/83.935033

[21] Li C, Kao CY, Gore JC, Ding Z. Implicit active contours driven by local binary fitting energy. In: IEEE Conference on Computer Vision and Pattern Recognition; 2007. pp. 1-7. doi: 10.1109/CVPR.2007.383014

[22] Wu Y, He C. A convex variational level set model for image segmentation. Signal Processing 2015; 106: 123-133.

[23] Akram F, Kim JH, Lee CG, Choi KN. Segmentation of regions of interest using active contours with SPF function. Computational and Mathematical Methods in Medicine 2015; 2015: 710326.

[24] Ali H, Badshah N, Chen K, Khan GA, Zikria N. Multiphase segmentation based on new signed pressure force functions and one level set function. Turkish Journal of Electrical Engineering and Computer Sciences 2017; 25: 2943-2955.

[25] Ancuti CO, Ancuti C. Single image dehazing by multi-scale fusion. IEEE Transactions on Image Processing 2013; 22: 3271-3282. doi: 10.1109/TIP.2013.2262284

[26] Zhang K, Zhang L, Song H, Zhou W. Active contours with selective local or global segmentation: a new formulation and level set method. Image and Vision Computing 2010; 28: 668-676.

[27] Zhang K, Song H, Zhang L. Active contours driven by local image fitting energy. Pattern Recognition 2010; 43: 1199-1206.

[28] Paragios N, Rachid D. Geodesic active regions and level set methods for supervised texture segmentation. International Journal of Computer Vision 2002; 46: 223-247. doi: 10.1023/A:1014080923068